applied sciences

MDPI

Article

Numerical Analysis of Seismic Pounding between Adjacent Buildings Accounting for SSI

Mehmet Eren Uz [1], Anna Jakubczyk-Gałczyńska [2] and Robert Jankowski [2,*]

[1] Department of Civil Engineering, Faculty of Engineering, Aydin Adnan Menderes University, Aydin 09010, Turkey
[2] Faculty of Civil and Environmental Engineering, Gdansk University of Technology, 80-233 Gdansk, Poland
* Correspondence: jankowr@pg.edu.pl

Abstract: The structural pounding caused by an earthquake may damage structures and lead to their collapse. This study is focused on the pounding between two adjacent asymmetric structures with different dynamic properties resting on the surface of an elastic half-space. An exploration of the relationship between the effects of the seismic analysis with the impact response to the torsional pounding between adjacent buildings under different SSI effects has been presented. In this paper, the authors have proposed a procedure for analyzing the response for adjacent buildings subjected to the pounding effects, considering systems with multiple degrees of freedom and modal equations of motion with four types of soil. All the calculations have been performed based on the fourth-order Runge–Kutta method. The novelty of the present study is related to the fact that the rigorous and approximate methods are used to examine the effects of pounding and SSI simultaneously. As a result, these two methods have been thoroughly investigated for both effects and the results have been compared. The results show that the approximate method produces results that are slightly different from those obtained by the rigorous direct integration method in the case of small SSI effects due to an increase in the pounding force. The efficiency of the method is also validated using numerical examples.

Keywords: seismic analysis; structural pounding; soil–structure interaction; earthquake; torsional response

Citation: Uz, M.E.; Jakubczyk-Gałczyńska, A.; Jankowski, R. Numerical Analysis of Seismic Pounding between Adjacent Buildings Accounting for SSI. *Appl. Sci.* **2023**, *13*, 3092. https://doi.org/10.3390/app13053092

Academic Editor: Maria Favvata

Received: 3 December 2022
Revised: 15 February 2023
Accepted: 24 February 2023
Published: 27 February 2023

1. Introduction

Seismic researchers have often observed collisions between adjacent buildings that are not sufficiently separated. This phenomenon, known as earthquake-induced structural pounding, may lead to minor damage at the points of interaction during moderate ground motions [1,2]. It may also cause serious damage to colliding structures and even result in their collapse during major earthquakes. Examples include the Loma Prieta earthquake in 1989 [3] or the Athens earthquake in 1999 [4], when many cases of structural pounding of buildings occurred. Three important aspects of a complex seismic analysis of structure–foundation systems (see [5]) include the frequency-dependent interaction forces, nonproportional damping of soil–structure interaction (SSI), liquefaction [6–10], and pounding responses of adjacent buildings. Earthquake-induced structural pounding between symmetric buildings has been investigated [11–15]. Numerous researchers have studied the effects of structural interactions by applying different structural models and using different models of collisions [16–20]. Numerous researchers have also analyzed the SSI of asymmetric buildings exposed to seismic excitations [21–25]. In contrast, pounding between adjacent asymmetric structures with different dynamic properties and incorporating SSI has not been sufficiently explored.

SSI problems (see [5,26]) have been addressed in the frequency domain by means of either a Fourier or a Laplace transform [27–29] to consider the frequency-dependent interaction forces. However, in frequency-domain analysis, only linear responses can be

considered. The soil springs and dashpots associated with the translational rocking and torsional modes of vibration can be satisfactorily calculated for typical multistory buildings in the time domain using frequency-independent expressions [30]. Employing traditional modal analysis methods to derive equivalent modal damping from the diagonal terms of the transformed damping matrix without examining the off-diagonal elements is one of the common approximate approaches for analyzing nonclassically damped systems. Certain conditions may lead to unacceptable errors in the response when off-diagonal terms are ignored in the transformed damping matrix [31]. Jui-Liang and Keh-Chyuan [32] verified the accuracy of the two degree-of-freedom (DOF) modal equations of motion for conserving nonproportional damping compared with that of the damped one-way asymmetric buildings.

A simplified modal response analysis was developed for engineering applications that do not require complicated calculations of the equivalent modal damping. The outcomes of a parametric investigation, conducted by varying the structural parameter values, have also been investigated in the previous studies of the authors [33,34]. The parametric study is beyond the scope of this paper, which focuses on considering the SSI and impact effects for rigorous and approximate methods. According to the results of the response analysis conducted by Uz and Hadi [33], the pounding of buildings during ground motion excitation has a considerable influence on the longitudinal behavior of the lighter structure. Simplifications of the modal analysis and investigations on pounding-involved structural responses have been proposed [31,33,35–37]. Studies have also been conducted on the earthquake-induced responses of colliding symmetric structures incorporating SSI. However, to the best of our knowledge, our study is the first exploration of the effect of SSI on the response of adjacent asymmetric buildings exposed to pounding, although some studies [38–41] investigated the pounding effect or SSI effects individually on adjacent buildings. Therefore, our main objective in this study was to investigate the relationship between the effects of the seismic analysis with the response to the torsional pounding between adjacent buildings under different SSI effects. Both the SSI and pounding effects have not been adequately researched in the past in terms of rigorous and approximate methodologies. In most cases, they were evaluated independently. The novelty of the present study is related to the fact that the rigorous and approximate methods are used to examine the effects of pounding and SSI simultaneously. As a result, these two methods have been thoroughly investigated for both effects and the results have been compared. The response analysis procedure has been developed for adjacent buildings subjected to pounding effects using multi-DOF modal equations of motion with four types of soil. The fourth-order Runge–Kutta method has been applied in all the calculations. The numerical examples have been used to validate the efficiency of the proposed method.

2. Theoretical Model Framework

The basic model for SSI that considers the effects of the pounding force on adjacent buildings has been used in this study.

2.1. Equation of Motion

Figure 1 shows a structural model of two adjacent buildings on a half-space with elastic properties.

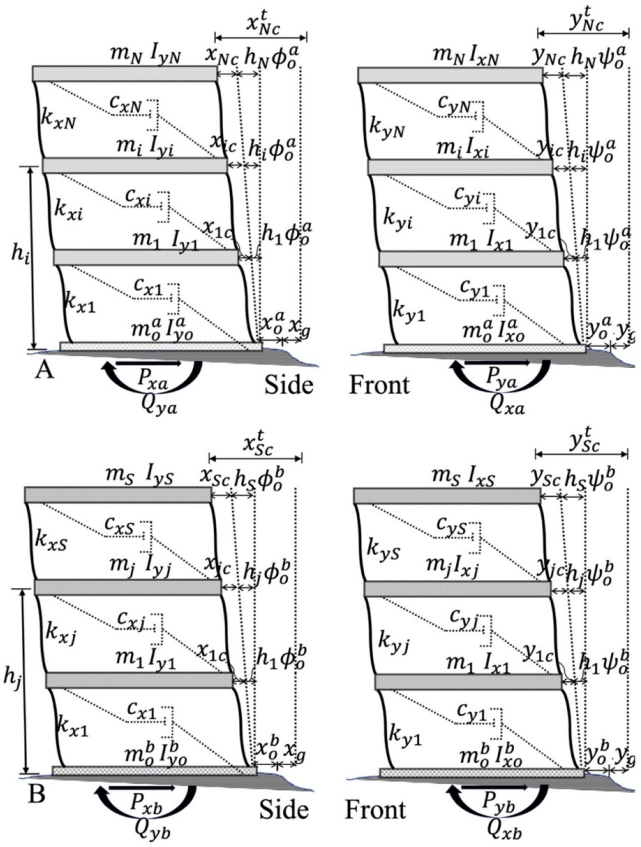

Figure 1. Modeling of asymmetric adjacent buildings.

Subscripts i and j in Figure 1 indicate the numbers of stories in the buildings. These are 1, 2, ..., N for Building A and 1, 2, ..., S for Building B. In this study, the following values have been determined: the mass, stiffness, damping coefficients, and moment of inertia of the floor with respect to the axes parallel to the x and y axes of Building A and in relation to the center of mass. In addition, Buildings A and B are represented either by the subscript or superscript a and b, respectively. A building with N stories has $3N + 5$ DOF; hence, Buildings A and B have $3N + 5$ and $3S + 5$ equations, respectively. Here, only the equations for Building A are highlighted. The equation of motion noted from previous studies [30,35,42–44] is briefly presented herein for completeness. The three equations of motion of each floor of the building may be written in a matrix form as (3 N):

$$\begin{aligned}
[M_a]\left\{\ddot{x}_{ic}^{t}\right\} + [C_{ax}]\{\dot{x}_i\} + [K_{ax}]\{x_i\} + \left[F_{xij}^{p}(t)\right] &= \{0\} \\
[M_a]\left\{\ddot{y}_{ic}^{t}\right\} + [C_{ay}]\{\dot{y}_i\} + [K_{ay}]\{y_i\} + \left[F_{yij}^{p}(t)\right] &= \{0\} \\
r_a^2[M_a]\left\{\ddot{\theta}_i^{t}\right\} + f_a[C_{ax}]\{\dot{x}_i\} - e_a[C_{ay}]\{\dot{y}_i\} + [C_{\theta R}^{a}]\left\{\dot{\theta}_{ic}\right\} + f_a[K_{ax}]\{x_i\} & \\
-e_a[K_{ay}]\{y_i\} + [K_{\theta R}^{a}]\{\theta_{ic}\} + \left[F_{\theta ij}^{p}(t)\right] &= \{0\}
\end{aligned} \tag{1}$$

The mass, damping, and stiffness of Building A in the submatrices are denoted as M_a, C_{ax}, C_{ay}, K_{ax}, and K_{ay}, in relation to both directions. These matrices are sized with $N \times N$ dimensions. As described by Equation (2), the parameters x_{ic}^{t}, y_{ic}^{t}, and θ_{ic}^{t} are the displacements of the center of mass of the floors along the longitudinal and transverse axes, and their twists about the upward axis (z) in Building A, respectively. The forces used for pounding in the longitudinal direction $F_{xij}^{p}(t)$ are obtained from the nonlinear viscoelastic model developed by Jankowski [45]. $F_{yij}^{p}(t)$ and $F_{\theta ij}^{p}(t)$ are derived by the Coulomb friction model used by Chopra [46]. The impact model (nonlinear viscoelastic model) is used in

this study for the rigorous model as it is. On the other hand, the impact model for the approximate method is deeply examined. x_i, y_i, and θ_{ic} are the displacement vectors of the center of resistance (CR) in the x and y directions and the twist of each floor with respect to the base, respectively. Additionally, two-way asymmetric buildings have been considered such that the CRs and center of masses (CMs) are not symmetrical along two axes of the horizontal plane as shown in Figure 2. The center of rigidity is the centroid of stiffness in a floor-diaphragm layout. The floor diaphragm experiences translational displacement in two directions and rotation when the center of stiffness is subjected to lateral loading.

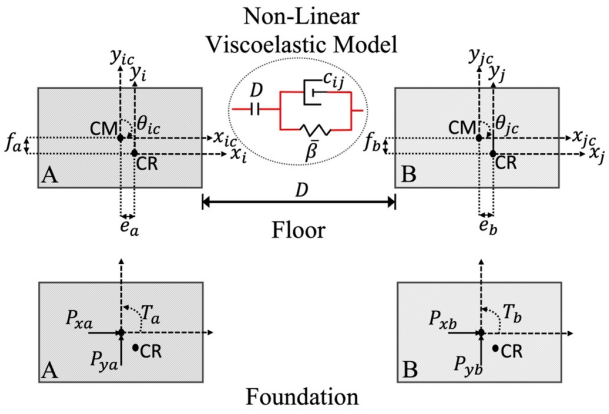

Figure 2. An asymmetric view of adjacent shear buildings in two directions.

The static eccentricity of the center of rigidity from the center of mass (e and f) for each story level does not differ, although the CR varies from floor to floor. Hence, the CR lies at the co-ordinates e_a, f_a of Building A and e_b, f_b of Building B. The radius of gyration of the floor mass is taken from the center of mass. The torsion stiffness matrix defined about the CR is denoted as $K^a_{\theta R}$, whereas $K^a_{\theta M}$ in Equation (1) is defined in relation to CM. Furthermore, the damping matrices of Building A are given as C_{ax}, C_{ay}, and $C^a_{\theta R}$, in Equation (1), considered proportionally to the stiffness matrices [47]. The displacement vectors of Building A in the related directions without the effects of SSI can be calculated as

$$\begin{gathered}\{x^t_{ic}\} = x^a_o\{1\} + x_g\{1\} + \varphi^a_o\{h_i\} + \{x_i\} - f_a\{\theta_{ic}\} \\ \{y^t_{ic}\} = y^a_o\{1\} + y_g\{1\} + \psi^a_o\{h_i\} + \{y_i\} + e_a\{\theta_{ic}\} \\ \{\theta^t_{ic}\} = \theta^a_o\{1\} + \{\theta_{ic}\}\end{gathered} \tag{2}$$

where x_i and y_i are vectors of displacement with relation to the CM of the superstructure; x^a_o, y^a_o, ψ^a_o, and ϕ^a_o represent the DOF at the foundation that is related to translations and rocking about the x and y axes; and θ^a_o is the rotation around the z axis. In each building, the five equations of motion of the foundation are described as translational and rocking distances in the x and y directions as well as a torsional mode of vibration.

2.2. Pounding Forces

The equation of motion for Building A can be expressed in terms of translation and rocking along the x and y axes and twist along the z axis, as described by Richart et al. [30], Sivakumaran and Balendra [23], and Jui-Liang et al. [35]. The static impedance functions have been used in this study (see [30]). Equation (3) shows the pounding-involved equation of motion for buildings with SSI:

$$\begin{bmatrix} M^a & 0 \\ 0 & M^b \end{bmatrix} \begin{Bmatrix} \ddot{U}^a(t) \\ \ddot{U}^b(t) \end{Bmatrix} + \begin{bmatrix} C^a & 0 \\ 0 & C^b \end{bmatrix} \begin{Bmatrix} \dot{U}^a(t) \\ \dot{U}^b(t) \end{Bmatrix} + \begin{bmatrix} K^a & 0 \\ 0 & K^b \end{bmatrix} \begin{Bmatrix} U^a(t) \\ U^b(t) \end{Bmatrix} + \begin{Bmatrix} F^p(t) \\ -F^p(t) \end{Bmatrix} = -\begin{Bmatrix} P^a(t) \\ P^b(t) \end{Bmatrix} \tag{3}$$

where $F^p(t)$, $P^a(t)$, and $P^b(t)$ are the vectors including the impact forces between floor masses (m_i, m_j).

In this study, the pounding force was simulated based on the nonlinear viscoelastic model [45,48–50].

2.3. Approximate Normal Modes of Adjacent Buildings

Equation (4) can be expressed in the following form, as proposed by Chopra and Goel [51]:

$$P^a(t) = \sum_{n=1}^{3N+5} s_n^a \left(\Gamma_{xn}^a \ddot{x}_g + \Gamma_{yn}^a \ddot{y}_g\right); P^b(t) = \sum_{n=1}^{3S+5} s_n^b \left(\Gamma_{xn}^b \ddot{x}_g + \Gamma_{yn}^b \ddot{y}_g\right) \quad (4)$$

The n^{th}-mode modal inertia force distribution can be calculated as $M^a\varphi_n^a$ for vector s_n^a and $M^b\varphi_n^b$ for vector s_n^b. The φ_n^a calculated from K^a and M^a is the n^{th}-mode shape without damping. φ_n^b is also obtained in the same way as φ_n^a. Γ_{xn}^a, Γ_{yn}^a, Γ_{xn}^b, and Γ_{yn}^b in the longitudinal and perpendicular directions for the n^{th} modal contribution values for both buildings. The output values of $U(t)$ contain translations in the x and y directions, rotations for each floor of the superstructure and the foundation, and the rocking angles for the foundation only in both directions. The n^{th} mode of the contribution factor in the modal analysis is calculated as

$$\begin{aligned} \Gamma_{xn}^a &= \frac{\varphi_n^{aT} \times M^a \times \left[\mathbf{1^T}\ \mathbf{0^T}\ \mathbf{0^T} 1\ 0\ 0\ 0\ 0\right]^T}{\varphi_n^{aT} \times M^a \times \varphi_n^a}; \\ \Gamma_{yn}^a &= \frac{\varphi_n^{aT} \times M^a \times \left[\mathbf{0^T}\ \mathbf{1^T}\ \mathbf{0^T} 0\ 1\ 0\ 0\ 0\right]^T}{\varphi_n^{aT} \times M^a \times \varphi_n^a} \end{aligned} \quad (5)$$

where **1** and **0** are the unit and zero vectors, respectively, sized as $N \times 1$. Equation (5) proves that the n^{th} modal participation factors rely on the path of the horizontal ground motion excitations. The 1940 El Centro (117 El Centro Array-9 station) and the 1995 Kobe (KJMA station) ground motions have been used for the analysis of both buildings, which is shown in Figure 3. The top accelerations of the related excitations were scaled to 0.3 g and 0.2 g for the 1940 El Centro NS-EW and 0.8 g and 0.6 g for the 1995 Kobe NS-EW, respectively.

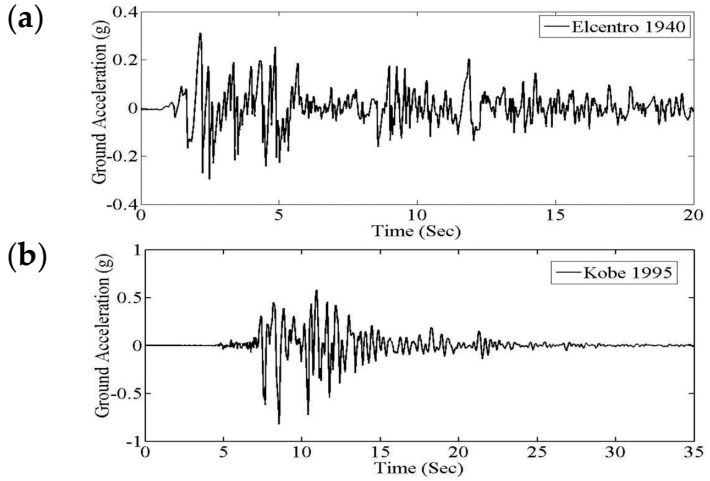

Figure 3. (**a**) 1940 El Centro and (**b**) 1995 Kobe earthquakes with maximum ground acceleration scaled to 0.3 g and 0.8 g, respectively.

U_n^a and U_n^b are defined in Equation (4) by the time variations in $\ddot{x}_g(t)$ and $\ddot{y}_g(t)$. In the analysis, the vertical motion of the ground was not in use. The force distribution can be expressed with the sum of the modal inertia forces, as given in Equation (4). T_n^a and T_n^b

are $(3N+5)\times 8$ and $(3S+5)\times 8$ diagonal matrices for both buildings, respectively. φ^a_{xn}, φ^a_{yn}, and $\varphi^a_{\theta n}$ in T^a_n are subvectors of the n^{th} natural vibration mode in the superstructure, sized as $N\times 1$. They are related to the displacement in both directions and the rotating DOF. $\phi^a_{x_o n}$, $\phi^a_{y_o n}$, $\phi^a_{\theta_o n}$, $\phi^a_{\psi_o n}$, and $\phi^a_{\phi_o n}$ in T^a_n are five subvectors of the mode shapes of the SSI system for Building A. With generalized modal co-ordinates for both buildings, the n^{th} undamped modal displacement responses, U^a_n and U^b_n, can be redefined as

$$\begin{Bmatrix} U^a_n(t) \\ U^b_n(t) \end{Bmatrix} = \begin{bmatrix} T^a_n & 0 \\ 0 & T^b_n \end{bmatrix} \begin{bmatrix} D^a_n(t) \\ D^b_n(t) \end{bmatrix} \tag{6}$$

where D^a_n and D^b_n are the n^{th} generalized modal co-ordinate of both buildings. By substituting Equation (6) and rearranging each side of the equation of motion by $\begin{bmatrix} T^a_n & 0 \\ 0 & T^b_n \end{bmatrix}^T$, we obtain

$$\begin{bmatrix} M^a_n & 0 \\ 0 & M^b_n \end{bmatrix} \begin{bmatrix} \ddot{D}^a_n(t) \\ \ddot{D}^b_n(t) \end{bmatrix} + \begin{bmatrix} C^a_n & 0 \\ 0 & C^b_n \end{bmatrix} \begin{bmatrix} \dot{D}^a_n(t) \\ \dot{D}^b_n(t) \end{bmatrix} + \begin{bmatrix} K^a_n & 0 \\ 0 & K^b_n \end{bmatrix} \begin{bmatrix} D^a_n(t) \\ D^b_n(t) \end{bmatrix} + \begin{bmatrix} F^{ap}_n(t) \\ -F^{bp}_n(t) \end{bmatrix} = -\begin{Bmatrix} M^a_n \iota \left(\Gamma^a_{xn} \ddot{x}_g + \Gamma^a_{yn} \ddot{y}_g \right) \\ M^b_n \iota \left(\Gamma^b_{xn} \ddot{x}_g + \Gamma^b_{yn} \ddot{y}_g \right) \end{Bmatrix} \tag{7}$$

where $M^a_n = T^{aT}_n M^a T^a_n$, $C^a_n = T^{aT}_n C^a T^a_n$, $K^a_n = T^{aT}_n K^a T^a_n$, $M^b_n = T^{bT}_n M^b T^b_n$, $C^b_n = T^{bT}_n C^b T^b_n$, and $K^b_n = T^{bT}_n K^b T^b_n$ are sized 8×8; ι is a vector sized as an 8×1 column with all elements the same as unity; the $3N+5$ and $3S+5$ multi-DOF modal equations of motion, as given in Equation (7) for both buildings, comprise a nonproportionally damped system.

$$\begin{aligned} C^a &= T^{aT}_n (\alpha M^a + \beta K^a) T^a_n = \alpha M^a_n + \beta K^a_n \\ C^b &= T^{bT}_n \left(\alpha M^b + \beta K^b \right) T^b_n = \alpha M^b_n + \beta K^b_n \end{aligned} \tag{8}$$

Cruz and Miranda [52] found that the Rayleigh damping model underestimates the damping of higher modes that contribute to the seismic response, resulting in an overestimation of the seismic response. This manuscript does not address the validity of the mass-proportional and stiffness-proportional assumptions in Rayleigh damping. The approximation approach and rigorous methods are contrasted in the first three modes of this study. If C^a and C^b are proportionally damped, i.e., $C^a = (\alpha M^a + \beta K^a)$ and $C^b = \left(\alpha M^b + \beta K^b \right)$, the n^{th} modal damping matrices for each building can be described as Equation (8). In here, α and β are coefficients found by the damping ratios of the two specific modes, since the original SSI system is not proportionally damped, i.e., $C^a \neq (\alpha M^a + \beta K^a)$, $C^b \neq \left(\alpha M^b + \beta K^b \right)$. In approximate method, Equation (8) converts $C^a \neq \alpha M^a_n + \beta K^a_n$ and $C^b \neq \alpha M^b_n + \beta K^b_n$ based on [35]. The nonlinear viscoelastic model is only modified for the approximate method used in this study, as given in Equation (9). Notably, the elements of D^a_n and D^b_n are not the same, even in an elastic state.

$$
\begin{gathered}
F^{p}_{xijn}(t) = 0 \text{ for } \delta_{ijxn}(t) \leq 0; \\
F^{p}_{xijn}(t) = \overline{\beta}\left(\delta_{ijxn}(t)\right)^{3/2} + \overline{c}_{ijn}(t)\dot{\delta}_{ijxn}(t) \text{ for } \delta_{ijxn}(t) > 0 \text{ and } \dot{\delta}_{ijxn}(t) > 0; \\
F^{p}_{xijn}(t) = \overline{\beta}\left(\delta_{ijxn}(t)\right)^{3/2} \text{ for } \delta_{ijxn}(t) > 0 \text{ and } \dot{\delta}_{ijxn}(t) \leq 0; \\
\delta_{ijxn}(t) = \delta_{ijyn}(t) = D^{a}_{xn}\varphi^{a}_{ixn}(t) - D^{b}_{xn}\varphi^{b}_{jxn}(t) - D;\ \delta_{ij\theta n}(t) = D^{a}_{\theta n}\varphi^{a}_{i\theta n}(t)f^{a} - \\
D^{b}_{\theta n}\varphi^{b}_{j\theta n}(t)f^{b} - D; \\
\dot{\delta}_{ijxn}(t) = \dot{D}^{a}_{xn}\varphi^{a}_{ixn}(t) - \dot{D}^{b}_{xn}\varphi^{b}_{jxn}(t);\ \dot{\delta}_{ijyn}(t) = \dot{D}^{a}_{yn}\varphi^{a}_{iyn}(t) - \dot{D}^{b}_{yn}\varphi^{b}_{jyn}(t); \\
\dot{\delta}_{ij\theta n}(t) = \dot{D}^{a}_{\theta n}\varphi^{a}_{i\theta n}(t)f^{a} - \dot{D}^{b}_{\theta n}\varphi^{b}_{j\theta n}(t)f^{b}; \\
F^{ap}_{ijn} = \left[F^{ap}_{xijn}\ F^{ap}_{yijn}\ F^{ap}_{\theta ijn}0\,0\,0\,0\,0\right]^{T}_{(3N+5)\times 1}
\end{gathered}
\tag{9}
$$

Here, $\delta_{ij}(t)$ is the total displacement between the buildings with respect to the foundation; $\dot{\delta}_{ij}(t)$ is their velocity; $\overline{\beta}$ is the damping; and $\overline{c}_{ij}(t)$ is the stiffness of the impact element. The damping ratio $(\overline{\xi})$ in relation to the coefficient of restitution (e) provides the dissipation of energy during impact [53]. D is the distance between the buildings. $F^{ap}_{\theta ijn}$ can be calculated as F^{ap}_{xijn} using the related $\delta_{ij\theta n}(t)$ and $\dot{\delta}_{ij\theta n}(t)$ in Equation (9). $F^{ap}_{n}(t) = T^{aT}_{n}F^{ap}_{ijn}$ in Equation (7) is an 8×1 vector with pounding forces. As a result, the approximate method substantially reduces the size of the matrices from $3\,N + 5$ to 8 for each building. The modal responses with regard to the displacement of each building, $D^{a}_{n}(t)$ and $D^{b}_{n}(t)$, are derived using the method of direct integration in Equation (7). The following equation is derived to obtain all the responses of the two nonproportionally damped asymmetric buildings on the top of an elastic half-space:

$$
U^{a}(t) = \sum_{n=1}^{3N+5} U^{a}_{n}(t) \approx \sum_{n=1}^{3N+5} T^{a}_{n}D^{a}_{n}(t); U^{b}(t) = \sum_{n=1}^{3S+5} U^{b}_{n}(t) \approx \sum_{n=1}^{3S+5} T^{b}_{n}D^{b}_{n}(t) \tag{10}
$$

The first few modal responses in Equation (10), to acquire a satisfying result, should be summed similarly to the displacement analysis.

2.4. Equation of Motion for SSI System

Based on Figure 1, the equation of motion for the entire foundation system for Building A can be derived from Equation (11) for the translation along the x and y axes, rotation around the z axis, and rocking along the x and y axes.

$$
\begin{gathered}
m^{a}_{o}\left(\ddot{x}_{g} + \ddot{x}^{a}_{o}\right) + \{1\}^{T}[M_{a}]\left\{\ddot{x}^{t}_{ic}\right\} + P_{xa}(t) = 0 \\
m^{a}_{o}\left(\ddot{y}_{g} + \ddot{y}^{a}_{o}\right) + \{1\}^{T}[M_{a}]\left\{\ddot{y}^{t}_{ic}\right\} + P_{ya}(t) = 0 \\
r^{2}_{a}m^{a}_{o}\ddot{\theta}^{a}_{o} + r^{2}_{a}\{1\}^{T}[M_{a}]\left\{\ddot{\theta}^{t}_{i}\right\} + T_{a}(t) = 0 \\
\sum_{i=0}^{N} I_{xi}\ddot{\psi}^{a}_{o} + \{h_{i}\}^{T}[M_{a}]\left\{\ddot{y}^{t}_{ic}\right\} + Q_{xa}(t) = 0 \\
\sum_{i=0}^{N} I_{yi}\ddot{\phi}^{a}_{o} + \{h_{i}\}^{T}[M_{a}]\left\{\ddot{x}^{t}_{ic}\right\} + Q_{ya}(t) = 0
\end{gathered}
\tag{11}
$$

The soil–structure interface has been modelled using a parallel set of frequency-independent springs and dashpots considered in the study of Richart et al. [30]. P_{xa}, P_{ya},

T_a, Q_{xa}, and Q_{xa} in Equation (11) are the interaction forces of Building A as given in Equation (12).

$$\begin{aligned} P_{xa}(t) &= C_T \dot{x}_o^a + K_T x_o^a \\ P_{ya}(t) &= C_T \dot{y}_o^a + K_T y_o^a \\ T_a(t) &= C_\theta \dot{\theta}_o^a + K_\theta \theta_o^a \\ Q_{xa}(t) &= C_\psi \dot{\psi}_o^a + K_\psi \psi_o^a \\ Q_{ya}(t) &= C_\phi \dot{\phi}_o^a + K_\phi \phi_o^a \end{aligned} \tag{12}$$

where $K_{T,\theta,\psi,\varnothing}$ and $C_{T,\theta,\psi,\varnothing}$ are the spring and dashpot coefficients of translations along both x and y axes, the torsion and rocking movements along both x and y axes, respectively. These constants of the static impedance functions are shown in Table 1 with many subscripts, as seen in Equation (12) [30].

Table 1. Spring and dashpot constants used by Richart et al. [30].

	Sliding	**Torsion**	**Rocking**
Spring	$K_T = \frac{32(1-v)Gr_o}{7-8v}$	$K_\theta = \frac{16Gr_o^3}{3}$	$K_{\psi,\phi} = \frac{8Gr_o^3}{3(1-v)}$
Mass Ratio	$B_T = \frac{(7-8v)M_T}{32(1-v)\rho r_o^3}$	$B_\theta = \frac{I_\theta}{\rho r_o^5}$	$B_{\psi,\phi} = \frac{3(1-v)I_{\psi,\phi}}{8\rho r_o^5}$
Damping Ratio	$D_T = \frac{0.288}{\sqrt{B_T}}$	$D_\theta = \frac{0.5}{1+2B_\theta}$	$D_{\psi,\phi} = \frac{0.15}{(1+B_{\psi,\phi})\sqrt{B_{\psi,\phi}}}$
Coefficient	$C_T = 2D_T\sqrt{K_T M_T}$	$C_\theta = 2D_\theta\sqrt{K_\theta I_\theta}$	$C_{\psi,\phi} = 2D_{\psi,\phi}\sqrt{K_{\psi,\phi} I_{\psi,\phi}}$

Where M_T, I_θ, and $I_{\psi,\phi}$ are the total mass, polar moment of inertia, and moment of inertia of the rigid body for rocking, respectively. G, ρ, v, and v_s are the shear modulus, mass density of half-space, Poisson's ratio, and shear velocity of the elastic medium, respectively. r_o is the radius of the massless disc on the surface of an elastic homogeneous half-space.

3. Numerical Study

In this study, five- and four-story asymmetric buildings are placed on an elastic half-space as Buildings A and B, respectively.

3.1. Structure Properties

Buildings A and B had the dimensions of 20 m by 15 m and 25 m by 20 m, respectively, with the longer lengths in the longitudinal direction (x) for each building. The ratio of the foundation mass to the floor mass was 3 for each building. Each story in each building was 2.85 m high. Table 2 provides the basic values describing the structural characteristics that have been used for this study.

Table 2. Building details [31,51].

Story No.	**Story Height** h_i, h_j **(m)**	**Building** A		**Building** B	
		$m_i \times 10^6$ **(kg)**	$k_i \times 10^8$ **(N/m)**	$m_j \times 10^6$ **(m)**	$k_j \times 10^8$ **(N/m)**
1F	2.85	0.30	3.46	0.4065	5.06
2F	5.7	0.30	3.46	0.4065	3.86
3F	8.55	0.30	3.46	0.4065	3.86
4F	11.4	0.30	3.46	0.4065	3.86
5F	14.25	0.30	3.46	-	-

Based on the reported results [34,54,55], we used $\overline{\beta} = 2.75 \times 10^9$ N/m$^{3/2}$ and $\overline{\xi} = 0.35$ for the pounding force parameters in the nonlinear viscoelastic model, with an established coefficient of friction $\left(\mu_f\right)$ of 0.5. In Equation (13), the translational and torsional stiffness

at the center of mass for each story of a building are longitudinally in proportion to the stiffness of the same story [56].

$$\beta_y = \frac{k_{yi}}{k_{xi}} = \frac{k_{yj}}{k_{xj}};\ \beta_t = \frac{k_{\theta i}}{r_a^2 k_{xi}} = \frac{k_{\theta j}}{r_b^2 k_{xj}} \tag{13}$$

The values of β_y and β_t were 1.32 and 1.69 for both buildings, respectively. Both buildings were characterized by 2% of the critical damping as a constant of proportionality (α) in the first vibration mode. Poisson's ratio (υ) was 0.333, and the density of the soil (ρ) was 1922 kg/m^3. Specifically, four types of soil at shear wave velocities ranging from 65, 130, 200, to 300 m/s as Case I to IV have been examined, respectively. These ranges are described as soft to hard soil, based on Abdel Raheem, et al. [57] and Sulistiawan et al. [58]. Soft soil (Case I) indicates the large SSI effect on the building's response, while hard soil (Case IV) indicates the small SSI effect. The original distance, D, between the buildings was 0.04 m. The selection of this value has been based on the previous studies [48,59,60]. A rigorous method using the direct integration method has been applied to compute the equation of motion for the responses of the SSI system of each building shown in Equation (1).

3.2. Response Analysis

The results have been compared with those reported by Balendra et al. [42], Sivakumaran and Balendra [23], and Jui-Liang et al. [35], who did not address the effect of pounding. As the reference building (RB) in this study, another four-story building without considering SSI has been chosen.

The first six natural frequencies of the eight-story building-foundation system used by Balendra et al. [42] are shown in Table 3. As can be seen from the table, the x-direction displacement component is dominant in the first and fourth modes, while the y-direction displacement component is dominant in the second and fifth modes. The major component in the third and sixth modes corresponds to the rotation around the vertical axis. Building B has a modal response that is less than that of Building A, but with the same trend; therefore, the results of Building B are not provided here. Figure 4 shows the mode shapes of Building A placed on rigid ground as well as the mode shapes of each case using the approximate method. The thin lines in Figure 4 represent the translations and rotations of the base, as shown by the offsets and slopes. In Figure 4, the first to third mode shapes of the dominant motions are the x- and y-translation and rotation around the vertical axis for both the RB without the effects of SSI and for all cases.

Table 3. First six natural frequencies of an eight-story building-foundation system considered in [38] compared with those in the current study.

Cases Frequency	Case I	Case I *	Case IV	Case IV *	RB	RB *	$\frac{\text{Case I *}}{\text{RB *}}$	$\frac{\text{Case IV *}}{\text{RB *}}$
W_1 (Hz)	0.698	0.685	0.788	0.787	0.794	0.792	0.865	0.994
W_2 (Hz)	0.783	0.787	0.932	0.931	0.941	0.940	0.837	0.990
W_3 (Hz)	1.120	1.107	1.224	1.222	1.233	1.231	0.899	0.993
W_4 (Hz)	1.896	1.874	1.942	1.937	1.943	1.941	0.965	0.998
W_5 (Hz)	2.227	2.175	2.301	2.297	2.306	2.303	0.944	0.997
W_6 (Hz)	2.905	2.795	3.013	3.007	3.019	3.015	0.927	0.997

* Obtained by current studies; RB: reference building.

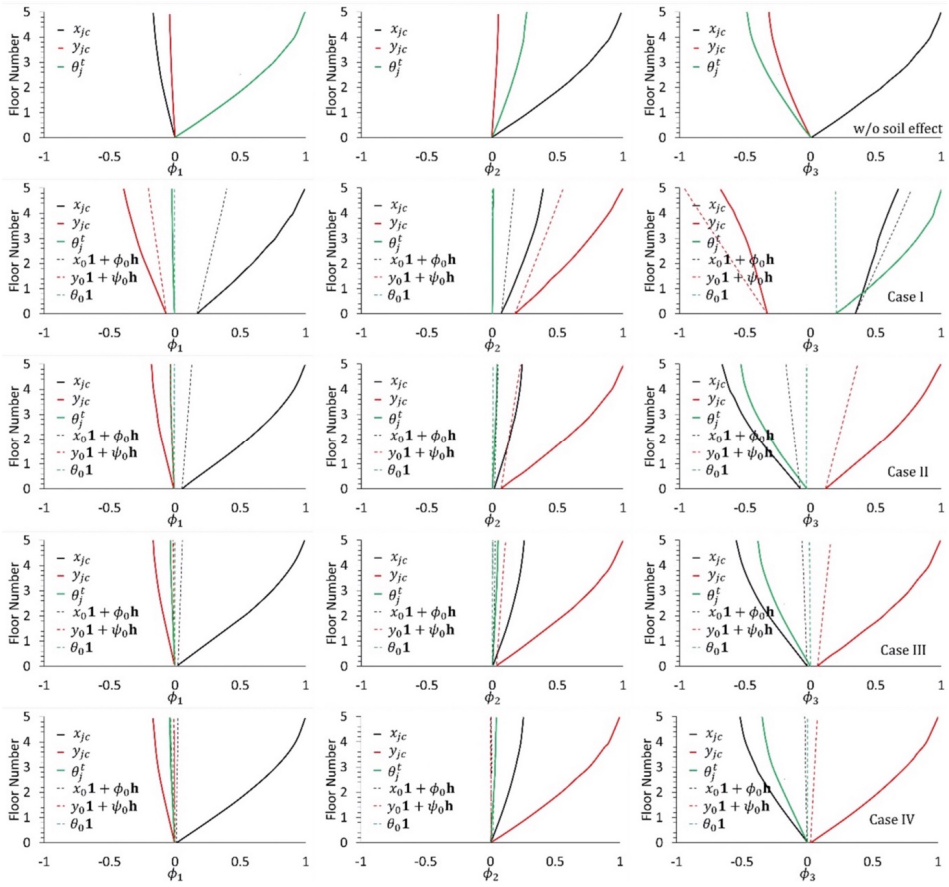

Figure 4. Building *A* in the first to third modes without considering SSI effects and for all cases.

However, the third mode shape in Case I is characterized by a rocking movement in the *y*-direction. In Cases I to IV, the first to third modes of shapes are consistent with those of the reference building. Figure 5 shows that the modal dislocation–time interactions for each of the eight DOFs for Case I are different.

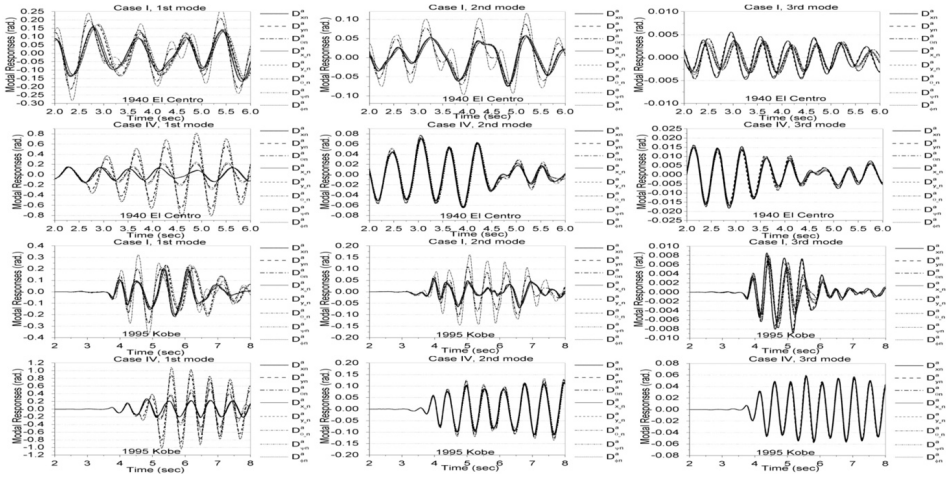

Figure 5. First to third modes during soft and hard soil earthquakes used in this study.

In Case IV, the modal responses for the eight DOFs display a similar pattern to those of the second and third modes. Case I shows that the modal responses for the first three modes are mainly affected by SSI effects, and they are out of phase. Figure 6 shows the response of the first mode in Case IV without any pounding.

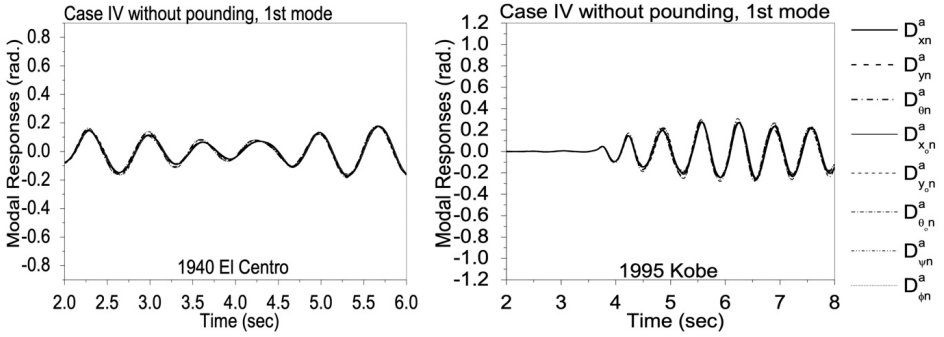

Figure 6. First-mode responses for El Centro earthquake in 1940 and Kobe earthquake in 1995 without pounding.

As shown in Figure 6, when the necessary distance is present between the buildings to avoid pounding, the modal responses of the eight DOFs for each vibration mode are similar to those in Case IV. Figure 7 illustrates the response histories of Cases I and IV obtained with the proposed method under the 1995 Kobe earthquake. The dashed line in Figure 7 denotes the approximate method (App.) given by Equation (7), whereas the solid line denotes the rigorous method (Rig.) obtained by Equation (3).

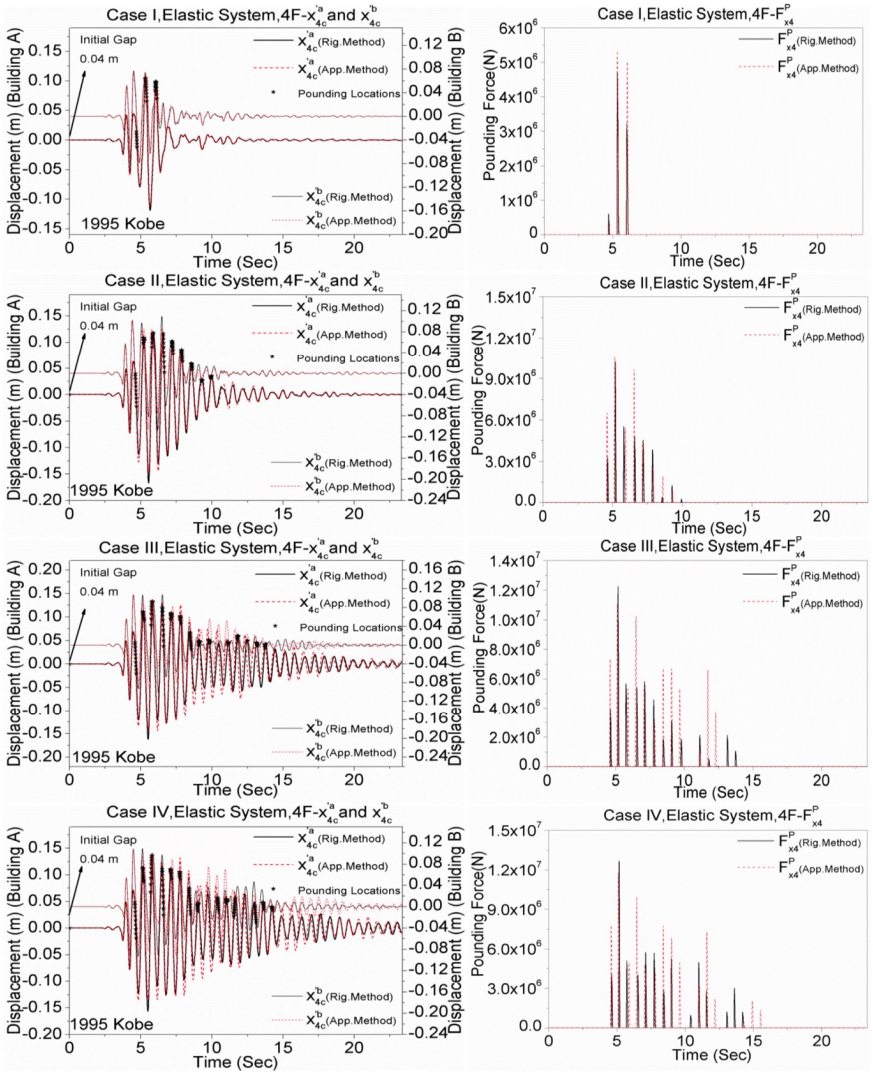

Figure 7. Results for both approximate and rigorous solutions on the fourth floor for the 1995 Kobe earthquake.

For Cases I and II, excellent agreement between the peak and phase responses for both methods has been found for the selected earthquakes. Notably, both methods produced slightly different response histories for the fourth story due to the larger forces under the small SSI effects, as shown in Figure 7. As a result of the high pounding forces in the first through third modes, the responses at the foundation obtained by the rigorous method in Figure 8 are not fully in agreement with those achieved by the approximate method in Case IV. Based on the comparison between the conventional rigorous method and the approximate method, it could be concluded that the approximate method markedly improves the accuracy of the analytical results without increasing the computational effort and by reducing the dimensions of the matrix.

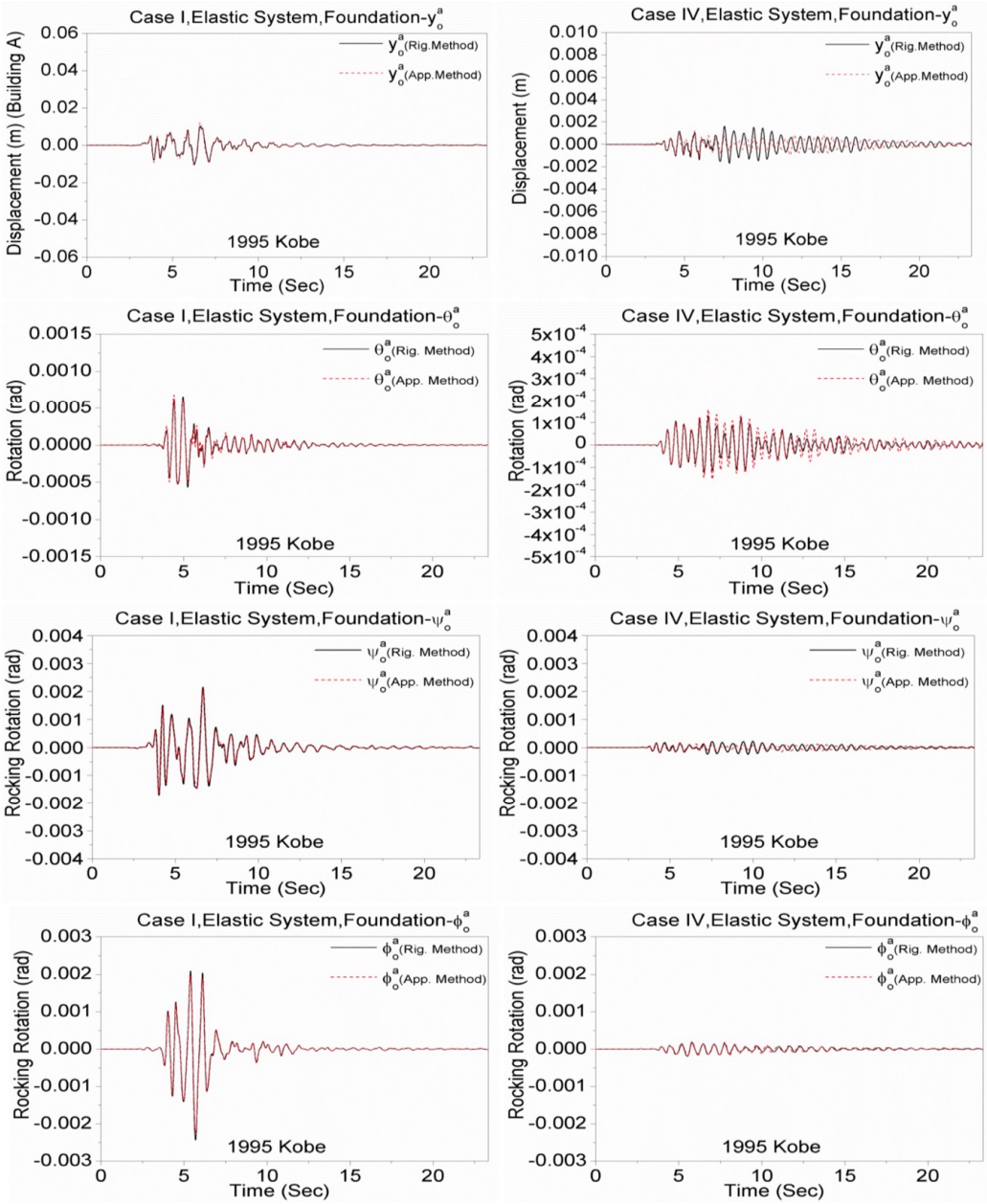

Figure 8. Time histories of Cases I and IV for the foundation during the 1995 Kobe earthquake.

Regarding the large SSI effect (Case I), both methods produced the same results for the 1995 Kobe earthquake in terms of translation, twisting, and rocking. Figure 9 compares both methods based on the story shears and torque with and without pounding. Figure 9 shows the maximum story shears in the x- and y-directions, together with the maximum

story torque in relation to the upright direction for shear waves traveling at 65 and 300 m/s. This is based on simulations by Balendra et al. [42,43]. For validation purposes, these two methods used in this study are compared with the findings of Balendra et al. [42,43] without considering the pounding effect.

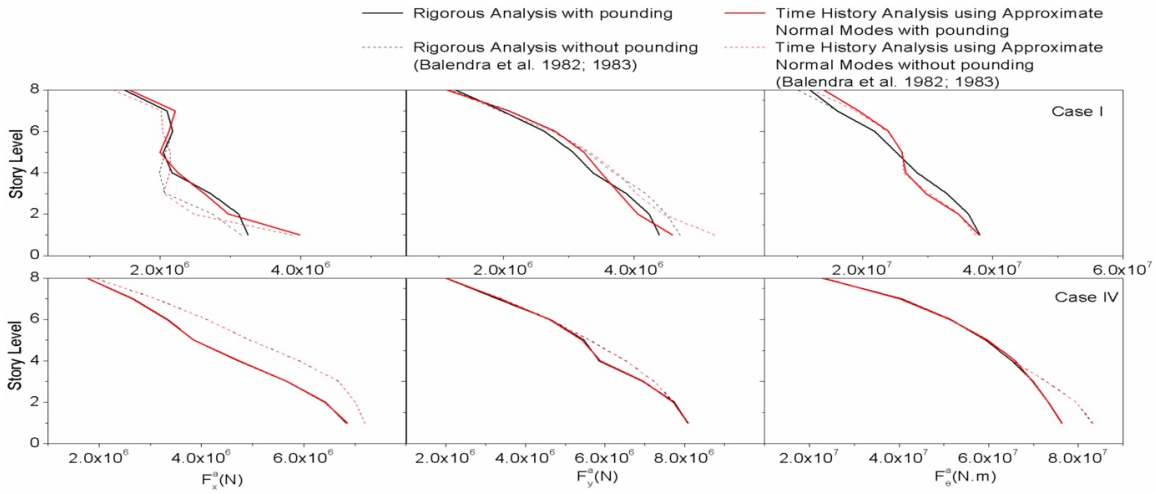

Figure 9. Maximum shear and torque of an eight-story building in Cases I and IV for the effects of pounding during the 1940 El Centro earthquake [42,43].

Based on the results for the large SSI case, the approximate and rigorous methods provided in Figure 9 for adjacent buildings are completely in agreement. Figure 9 also shows that, in Case IV, the maximum responses to the story shear and torque are reduced due to reduced pounding.

Abdel Raheem [61] has studied the bi-directional excitation and biaxial interaction of the base isolation system, although there is still debate on the base isolation system's behavior under the SSI and hammering impacts. Two approaches utilized in this study will be applied to base-isolated buildings on various soil types, taking impact effects into account.

4. Conclusions

In this study, the seismic behavior of multistory asymmetric adjacent buildings by considering SSI and structural pounding has been examined. The effects of the pounding force on the adjacent structures in a simplified model have been considered. The parallel set of frequency-independent springs and dashpots to simulate the interaction forces at the SSI has been applied. The fourth-order Runge–Kutta differential equations for two-way asymmetric shear buildings have been derived, which have been solved both with and without impacts. The approximate method using multi-DOF modal equations of motion and the rigorous method using direct integration have been compared.

The SSI has been incorporated to generate a set of modal equations of motion for the pounding responses for each building based on the frequency-independent equation of motion. The results of this study indicated that pounding detrimentally affects the dynamic properties of a building. Because the shear wave velocity is very low, the approximate method produces the same impact force as the rigorous method. However, these findings are not valid for small SSI effects due to the increased number of collisions. The response to small SSI effects at the foundation is less than that to large SSI effects. The top floor deformations of adjacent buildings are somewhat conservative at a high shear wave velocity. Finally, buildings are considerably affected by increased shear wave velocity. All the vibration modes, rather than only the first few vibration modes, should be considered to achieve satisfactory results.

The simultaneous effects of SSI and the pounding of adjacent buildings under seismic loading have not been assessed so far by the use of the approximate and rigorous method.

Both methods only evaluated the cases showing the SSI effect in the past. By comparing the SSI and pounding effects in these two techniques, the originality of this work has been demonstrated. It is vital to simulate colliding structures as inelastically as feasible in order to limit the consequences of pounding between buildings. By increasing the shear wave velocity, the responses, based on the deformation vectors for each structure, are drastically decreased while the SSI forces at the building's foundation are enhanced. In order to determine the efficacy of these approaches in different circumstances, further studies should compare them to standard isolated buildings using a sensitivity analysis.

Author Contributions: Conceptualization, M.E.U.; methodology, M.E.U., A.J.-G. and R.J.; software, M.E.U.; validation, M.E.U.; formal analysis, M.E.U.; investigation, M.E.U., A.J.-G. and R.J.; writing—original draft preparation, M.E.U.; writing—review and editing, A.J.-G. and R.J. All authors have read and agreed to the published version of the manuscript.

Funding: The authors declare that no funds, grants, or other support was received during the preparation of this manuscript.

Institutional Review Board Statement: Not applicable.

Informed Consent Statement: Not applicable.

Data Availability Statement: The datasets generated and analyzed during the current study are available upon request.

Acknowledgments: The authors would like to thank Muhammad N.S. Hadi for help in the interpretation of the databases and for providing a working space at the University of Wollongong, Australia.

Conflicts of Interest: The authors have no relevant financial or nonfinancial interest to disclose.

Notations

A	symbolized Building A
a_0	dimensionless frequency
B	symbolized Building B
B_T, $B_{\psi,\phi}$, B_θ	mass ratios for sliding, rocking, and torsion
C^a, C^b	damping matrices of the SSI system for each building
C_{ax}, C_{ay}	$N \times N$ submatrices of damping in x- and y-axis for Building A
c_{xi}, c_{yi}	ith floor damping coefficient in the longitudinal and transverse directions for Building A
c_{xj}, c_{yj}	jth floor damping coefficient in the longitudinal and transverse directions for Building B
$\bar{c}_{ij}$	damping of impact element
CM, CR	center of mass and resistance
$C^a_{\theta R}$, $C^a_{\theta M}$	torsional damping matrices of Building A in relation to CR and CM
C_T, $C_{\psi,\phi}$, C_θ	damping of soil dashpots
D	distance between buildings
D_T, $D_{\psi,\phi}$, D_θ	damping ratio of soil dashpots
e	coefficient of restitution
e_a, e_b	eccentricity in x-direction of Buildings A and B
$\{\boldsymbol{e_a}\}$, $\{\boldsymbol{e_b}\}$	$N \times 1$ column vector with all elements equal to e_a, e_b
$F^p(t)$	pounding force vector
F^p_{xij}, F^p_{yij}, $F^p_{\theta ij}$	pounding force influence coefficient vectors in longitudinal, transverse, and vertical directions
$F_a(t)$, $F_b(t)$	shear force matrices of SSI system for each building
F_{xi}, F_{yi}, $F_{\theta i}$	shear force of ith floor
F^y_{xi}, F^y_{yi}	yield strength of ith floor
f_a, f_b	eccentricity in y-direction of Buildings A and B
$\{\boldsymbol{f_a}\}$, $\{\boldsymbol{f_b}\}$	$N \times 1$ column vector with all elements equal to f_a, f_b

f_{max}	maximum wave frequency
G	shear modulus of soil
h_i, h_j	height of ith and jth floor level
$\{h_i\}$, $\left\{h_j\right\}$	column vector composed of story heights
I_{xi}, I_{yi}, I_{xj}, I_{yj}	moments of inertia of ith and jth floors
I^a_{x0}, I^a_{y0}, I^b_{x0}, I^b_{y0}	moments of inertia of the base for each building
I_θ, $I_{\psi,\phi}$	polar moment of inertia and moment of inertia for rocking of each building
K^a, K^b	stiffness matrices of SSI system for each building
K_{ax}, K_{ay}	$N \times N$ submatrices of stiffness in x- and y-axis for Building A
k_{xi}, k_{yi}	ith floor stiffness coefficient in longitudinal and transverse directions for Building A
k_{xj}, k_{yj}	jth floor stiffness coefficient in longitudinal and transverse directions for Building B
$K^a_{\theta R}$, $K^a_{\theta M}$	torsional stiffness matrices of Building A in relation to CR and CM
K_T, $K_{\psi,\phi}$, K_θ	stiffness of soil springs
M^a, M^b	generalized mass matrix of SSI systems of each building
M_T	mass of related building
M_a	mass matrix of superstructure
m_i	mass at ith floor of Building A
m_j	mass at jth floor of Building B
m^a_0, m^b_0	foundation masse
N	number of stories of Building A
$P^a(t)$, $P^b(t)$	loading vector of SSI system
P_{ax}, P_{ay}, P_{bx}, P_{by}	SSI forces
Q_{xa}, Q_{ya}, Q_{xb}, Q_{yb}	SSI moments
r_a, r_b	radius of gyration in relation to mass center
r_0	radius of a circle having same area as building plan
S	number of stories of Building B
T_a, T_b	SSI torques of buildings
t	time variable
U^a, U^b	deformation vector of Buildings A and B
V_s	shear wave velocity of soil
x'_{ic}, y'_{ic}, x'_{jc}, y'_{jc}	x- and y-directional displacement vectors of buildings with SSI effects
x_{ic}, y_{ic}, x_{jc}, y_{jc}	x- and y-directional displacement vectors of buildings without SSI effects
x^t_{ic}, y^t_{ic}, x^t_{jc}, y^t_{jc}	total displacement vectors of center mass of floors
x^a_0, y^a_0, x^b_0, y^b_0	x- and y-directional displacements of foundations of buildings
$\ddot{x}_g$, $\ddot{y}_g$	ground acceleration records
α	constant for determining classical damping
β	impact stiffness parameter
θ^t_i, θ_{ic}	rotational vector of building with and without SSI effects
δ_{ij}	relative displacement influence coefficient with respect to ground
$\dot{\delta}_{ij}$	relative velocity influence coefficient with respect to ground
Δt	time step
$\overline{\beta}$	damping ratio related to e
μ_f	friction coefficient during collision
ω_f	circular frequency of applied excitation
$\{\mathbf{1}\}$	$N \times 1$ or $S \times 1$ column vector with all elements equal to 1
$\mathbf{0}$	vector of zeros

References

1. Zembaty, Z.; Cholewicki, A.; Jankowski, R.; Szulc, J. Trzęsienia ziemi 21 września 2004 r. w Polsce północno-wschodniej oraz ich wpływ na obiekty budowlane (Earthquakes of September 21, 2004 in north-eastern Poland and their effects on structures). *Inżynieria I Bud.* **2005**, *61*, 3–9. (In Polish)
2. Zembaty, Z.; Jankowski, R.; Cholewicki, A.; Szulc, J. Trzęsienie ziemi 30 listopada 2004 r. na Podhalu oraz jego wpływ na obiekty budowlane (Earthquake of November 30, 2004 in Podhale and its effects on structures). *Inżynieria I Bud.* **2005**, *61*, 507–511. (In Polish)

3. Kasai, K.; Maison, B.F. Building pounding damage during the 1989 Loma Prieta earthquake. *Eng. Struct.* **1997**, *19*, 195–207. [CrossRef]
4. Vasiliadis, L.; Elenas, A. Performance of school buildings during the Athens earthquake of 7 September 1999. In Proceedings of the 12th European Conference on Earthquake Engineering, London, UK, 9–13 September 2002.
5. Kamgar, R.; Tavakoli, R.; Rahgozar, P.; Jankowski, R. Application of discrete wavelet transform in seismic nonlinear analysis of soil–structure interaction problems. *Earthq. Spectra* **2021**, *37*, 1980–2012. [CrossRef]
6. Karafagka, S.; Fotopoulou, S.; Pitilakis, D. Fragility assessment of non-ductile RC frame buildings exposed to combined ground shaking and soil liquefaction considering SSI. *Eng. Struct.* **2021**, *229*, 111629. [CrossRef]
7. Duan, W.; Congress, S.S.C.; Cai, G.; Liu, S.; Dong, X.; Chen, R.; Liu, X. A hybrid GMDH neural network and logistic regression framework for state parameter–based liquefaction evaluation. *Can. Geotech. J.* **2021**, *99*, 1801–1811. [CrossRef]
8. Özcebe, A.G.; Giretti, D.; Bozzoni, F.; Fioravante, V.; Lai, C.G. Centrifuge and numerical modelling of earthquake-induced soil liquefaction under free-field conditions and by considering soil-structure interaction. *Bull. Earthq. Eng.* **2021**, *19*, 47–75. [CrossRef]
9. Duan, W.; Zhao, Z.; Cai, G.; Pu, S.; Liu, S.; Dong, X. Evaluating model uncertainty of an in situ state parameter-based simplified method for reliability analysis of liquefaction potential. *Comput. Geotech.* **2022**, *151*, 104957. [CrossRef]
10. Madabhushi, G.S.P.; Garcia-Torres, S. Sustainable measures for protection of structures against earthquake induced liquefaction. *Indian Geotech. J.* **2021**, *51*, 467–481. [CrossRef]
11. Anagnostopoulos, S.A. Pounding of buildings in series during earthquakes. *Earthq. Eng. Struct. Dyn.* **1988**, *16*, 443–456. [CrossRef]
12. Flenga, M.G.; Favvata, M.J. Fragility Curves and Probabilistic Seismic Demand Models on the Seismic Assessment of RC Frames Subjected to Structural Pounding. *Appl. Sci.* **2021**, *11*, 8253. [CrossRef]
13. Kazemi, F.; Mohebi, B.; Jankowski, R. Predicting the seismic collapse capacity of adjacent SMRFs retrofitted with fluid viscous dampers in pounding condition. *Mech. Syst. Signal Process.* **2021**, *161*, 107939. [CrossRef]
14. Miari, M.; Jankowski, R. Incremental dynamic analysis and fragility assessment of buildings founded on different soil types experiencing structural pounding during earthquakes. *Eng. Struct.* **2022**, *252*, 113118. [CrossRef]
15. Polycarpou, P.C.; Papaloizou, L.; Komodromos, P. An efficient methodology for simulating earthquake-induced 3D pounding of buildings. *Earthq. Eng. Struct. Dyn.* **2014**, *43*, 985–1003. [CrossRef]
16. Chau, K.T.; Wei, X.X. Pounding of structures modelled as non-linear impacts of two oscillators. *Earthq. Eng. Struct. Dyn.* **2001**, *30*, 633–651. [CrossRef]
17. Favvata Maria, J.; Karayannis Chris, G.; Liolios Asterios, A. Influence of exterior joint effect on the inter-story pounding interaction of structures. *Struct. Eng. Mech.* **2009**, *33*, 113–136. [CrossRef]
18. Jing, H.-S.; Young, M. Impact interactions between two vibration systems under random excitation. *Earthq. Eng. Struct. Dyn.* **1991**, *20*, 667–681. [CrossRef]
19. Kazemi, F.; Miari, M.; Jankowski, R. Investigating the effects of structural pounding on the seismic performance of adjacent RC and steel MRFs. *Bull. Earthq. Eng.* **2021**, *19*, 317–343. [CrossRef]
20. Khatami, S.M.; Naderpour, H.; Barros, R.C.; Jakubczyk-Gałczyńska, A.; Jankowski, R. Determination of Peak Impact Force for Buildings Exposed to Structural Pounding during Earthquakes. *Geosciences* **2020**, *10*, 18. [CrossRef]
21. Balendra, T. A simplified model for lateral load analysis of asymmetrical buildings. *Eng. Struct.* **1983**, *5*, 154–162. [CrossRef]
22. Novak, M.; Hifnawy, L.E. Effect of soil-structure interaction on damping of structures. *Earthq. Eng. Struct. Dyn.* **1983**, *11*, 595–621. [CrossRef]
23. Sivakumaran, K.S.; Balendra, T. Seismic analysis of asymmetric multistorey buildings including foundation interaction and P-Δ effects. *Eng. Struct.* **1994**, *16*, 609–624. [CrossRef]
24. Uz, M.E.; Hadi, M.N.S. Optimal design of semi active control for adjacent buildings connected by MR damper based on integrated fuzzy logic and multi-objective genetic algorithm. *Eng. Struct.* **2014**, *69*, 135–148. [CrossRef]
25. Hadi, M.N.S.; Uz, M.E. Investigating the optimal passive and active vibration controls of adjacent buildings based on performance indices using genetic algorithms. *Eng. Optim.* **2015**, *47*, 265–286. [CrossRef]
26. Miari, M.; Choong, K.K.; Jankowski, R. Seismic Pounding Between Bridge Segments: A State-of-the-Art Review. *Arch. Comput. Methods Eng.* **2021**, *28*, 495–504. [CrossRef]
27. Chopra, A.K.; Gutierrez, J.A. Earthquake response analysis of multistorey buildings including foundation interaction. *Earthq. Eng. Struct. Dyn.* **1974**, *3*, 65–77. [CrossRef]
28. Gupta, V.K.; Trifunac, M.D. Seismic response of multistoried buildings including the effects of soil-structure interaction. *Soil Dyn. Earthq. Eng.* **1991**, *10*, 414–422. [CrossRef]
29. Veletsos, A.S.; Meek, J.W. Dynamic behaviour of building-foundation systems. *Earthq. Eng. Struct. Dyn.* **1974**, *3*, 121–138. [CrossRef]
30. Richart, F.E.; Hall, J.R.; Woods, R.D. *Vibrations of Soils and Foundations*; Prentice-Hall: Englewood Cliffs, NJ, USA, 1970.
31. Goel, R.K. Simplified analysis of asymmetric structures with supplemental damping. *Earthq. Eng. Struct. Dyn.* **2001**, *30*, 1399–1416. [CrossRef]
32. Lin, J.-L.; Tsai, K.-C. Simplified seismic analysis of one-way asymmetric elastic systems with supplemental damping. *Earthquake Eng. Struct. Dyn.* **2007**, *36*, 783–800. [CrossRef]

33. Uz, M.; Hadi, M.N. Investigating the effects of pouding for inelastic base isolated adjacent buildings under earthquake excitations. In *Incorporating Sustainable Practice in Mechanics of Structures and Materials*; Fragomeni, S., Venkatesan, S., Lam, N., Setunge, S., Eds.; CRC Press: Leiden, The Netherlands, 2011; pp. 329–334.
34. Jankowski, R.; Mahmoud, S. *Earthquake-Induced Structural Pounding*; Springer: Cham, Switzerland, 2015.
35. Lin, J.-L.; Tsai, K.-C.; Miranda, E. Seismic History Analysis of Asymmetric Buildings with Soil–Structure Interaction. *J. Struct. Eng.* **2009**, *135*, 101–112. [CrossRef]
36. Migda, W.; Szczepański, M.; Lasowicz, N.; Jakubczyk-Gałczyńska, A.; Jankowski, R. Non-Linear Analysis of Inter-Story Pounding between Wood-Framed Buildings during Ground Motion. *Geosciences* **2019**, *9*, 488. [CrossRef]
37. Favvata, M.J. Minimum required separation gap for adjacent RC frames with potential inter-story seismic pounding. *Eng. Struct.* **2017**, *152*, 643–659. [CrossRef]
38. Abdel Raheem, S.E. Mitigation measures for earthquake induced pounding effects on seismic performance of adjacent buildings. *Bull. Earthq. Eng.* **2014**, *12*, 1705–1724. [CrossRef]
39. Raheem, S.E.A.; Alazrak, T.M.A.; Shafy, A.G.A.A.; Ahmed, M.M.; Gamal, Y.A.S. Seismic pounding between adjacent buildings considering soil-structure interaction. *Earthq. Struct.* **2021**, *20*, 55–70. [CrossRef]
40. Abdel Raheem, S.; Fooly, M.; Shafy, A.; Abbas, Y.; Omar, M.; Latif, M.; Mahmoud, S. Seismic Pounding Effects on Adjacent Buildings in Series with Different Alignment Configurations. *Steel Compos. Struct.* **2018**, *28*, 289–308. [CrossRef]
41. Abdel Raheem, S.; Fooly, M.; Omar, M.; Abdel Zaher, A. Seismic pounding effects on the adjacent symmetric buildings with eccentric alignment. *Earthq. Struct.* **2019**, *16*, 715–726. [CrossRef]
42. Balendra, T.; Tat, C.W.; Lee, S.-L. Modal damping for torsionally coupled buildings on elastic foundation. *Earthq. Eng. Struct. Dyn.* **1982**, *10*, 735–756. [CrossRef]
43. Balendra, T.; Tat, C.W.; Lee, S.L. Vibration of Asymmetrical Building‐Foundation Systems. *J. Eng. Mech.* **1983**, *109*, 430–449. [CrossRef]
44. Flenga, M.G.; Favvata, M.J. Probabilistic seismic assessment of the pounding risk based on the local demands of a multistory RC frame structure. *Eng. Struct.* **2021**, *245*, 112789. [CrossRef]
45. Jankowski, R. Impact Force Spectrum for Damage Assessment of Earthquake-Induced Structural Pounding. *Key Eng. Mater.* **2005**, *293–294*, 711–718. [CrossRef]
46. Chopra, A.K. *Dynamics of Structures*; Prentice-Hall: Englewood Cliffs, NJ, USA, 1995.
47. Clough, R.W.; Penzien, J. *Dynamics of Structures*, 2nd ed.; McGraw-Hill Book Co., Inc.: New York, NY, USA, 1993.
48. Jankowski, R. Theoretical and experimental assessment of parameters for the non-linear viscoelastic model of structural pounding. *J. Theor. Appl. Mech.* **2007**, *45*, 931–942.
49. Hosseini, S.H.; Naderpour, H.; Vahdani, R.; Jankowski, R. Evaluation of pounding effects between reinforced concrete frames subjected to far-field earthquakes in terms of damage index. *Bull. Earthq. Eng.* **2022**, *20*, 1219–1245. [CrossRef]
50. Hadi, M.N.S.; Uz, M.E. Inelastic Base Isolated Adjacent Buildings under Earthquake Excitation with the Effect of Pounding. In Proceedings of the 5th Civil Engineering Conference in the Asian Region and Australasian Structural Engineering Conference CECAR 5/ASEC 2010, Sydney, Australia, 8–12 August 2010; pp. 155–201.
51. Chopra, A.K.; Goel, R.K. A modal pushover analysis procedure to estimate seismic demands for unsymmetric-plan buildings. *Earthq. Eng. Struct. Dyn.* **2004**, *33*, 903–927. [CrossRef]
52. Cruz, C.; Miranda, E. Evaluation of the Rayleigh damping model for buildings. *Eng. Struct.* **2017**, *138*, 324–336. [CrossRef]
53. Goldsmith, W. *Impact: The Theory and Physical Behaviour of Colliding Solids*; Edward Arnold: London, UK, 1960.
54. Uz, M.E.; Hadi, M.N.S. Seismic history analysis of asymmetrical adjacent buildings with soil-structure interaction con-sideration. In Proceedings of the 8th World Conference on Earthquake Resistant Engineering Structures, Chianciano, Italy, 7–9 September 2011; pp. 225–236.
55. Uz, M.E.; Hadi, M.N.S. *Earthquake Resistant Design of Buildings*, 1st ed.; CRC Press: Boca Raton, FL, USA, 2017. [CrossRef]
56. Kan, C.L.; Chopra, A.K. *Coupled Lateral Torsional Response of Buildings to Ground Motion*; University of California: Berkeley, CA, USA, 1976.
57. Abdel Raheem, S.E.; Ahmed, M.M.; Alazrak, T.M.A. Evaluation of soil–foundation–structure interaction effects on seismic response demands of multi-story MRF buildings on raft foundations. *Int. J. Adv. Struct. Eng.* **2015**, *7*, 11–30. [CrossRef]
58. Sulistiawan, H.; Supriyadi; Yulianti, I. Shear wave velocity profiling analysis for site classification using microtremor single station method. *AIP Conf. Proc.* **2018**, *2014*, 020003. [CrossRef]
59. Khatami, S.M.; Naderpour, H.; Razavi, S.M.N.; Barros, R.C.; Sołtysik, B.; Jankowski, R. An ANN-Based Approach for Prediction of Sufficient Seismic Gap between Adjacent Buildings Prone to Earthquake-Induced Pounding. *Appl. Sci.* **2020**, *10*, 3591. [CrossRef]

60. Khatami, S.M.; Naderpour, H.; Barros, R.C.; Jankowski, R. Verification of Formulas for Periods of Adjacent Buildings Used to Assess Minimum Separation Gap Preventing Structural Pounding during Earthquakes. *Adv. Civ. Eng.* **2019**, *2019*, 9714939. [CrossRef]
61. Abdel Raheem, S.E. Exploring Seismic Response of Bridges with Bidirectional Coupled Modelling of Base Isolation Bearings System. *Arab. J. Sci. Eng.* **2014**, *39*, 8669–8679. [CrossRef]